Space Weathering of Small Koronis Family Members

Cristina A. Thomas [a,e], Andrew S. Rivkin [b,e],

David E. Trilling [a,e], Marie-therese Enga [a,c,e], and

Jennifer A. Grier [d,e]

[a] *Northern Arizona University, Department of Physics and Astronomy, PO Box 6010 Flagstaff, AZ 86011*

[b] *Johns Hopkins University Applied Physics Laboratory, 11100 Johns Hopkins Road, Laurel, MD 20723*

[c] *Current Address: Arkansas Center for Space and Planetary Sciences, University of Arkansas 202 Old Museum Building, Fayetteville, AR 72701*

[d] *Planetary Science Institute, 1700 E. Fort Lowell Rd. Suite 106, Tucson, AZ 85719*

[e] *Visiting Astronomer, Kitt Peak National Observatory, National Optical Astronomy Observatory, which is operated by the Association of Universities for Research in Astronomy (AURA) under cooperative agreement with the National Science Foundation.*

Number of pages: 29

Number of tables: 2

Number of figures: 3

Preprint submitted to Icarus *17 December 2010*

Proposed Running Head:

Space Weathering of Small Koronis Family Members

Editorial Correspondence to:

Cristina A. Thomas

Northern Arizona University

Department of Physics and Astronomy

PO Box 6010

Flagstaff, AZ 86011 USA.

Email: cristina.thomas@nau.edu

Phone: (928) 523-9254

ABSTRACT

The space weathering process and its implications for the relationships between S- and Q-type asteroids and ordinary chondrite meteorites is an often debated topic in asteroid science. Q-type asteroids have been shown to display the best spectral match to ordinary chondrites (McFadden et al. 1985). While the Q-types and ordinary chondrites share some spectral features with S-type asteroids, the S-types have significantly redder spectral slopes than the Q-types in visible and near-infrared wavelengths. This reddening of spectral slope is attributed to the effects of space weathering on the observed surface composition. The analysis by Binzel et al. (2004) provided a missing link between the Q- and S-type bodies in near-Earth space by showing a reddening of spectral slope in objects from 0.1 to 5 km that corresponded to a transition from Q-type to S-type asteroid spectra, implying that size, and therefore surface age, is related to the relationship between S- and Q-types. The existence of Q-type asteroids in the main-belt was not confirmed until Mothé-Diniz and Nesvorný (2008) found them in young S-type clusters. The young age of these families suggest that the unweathered surface could date to the formation of the family. This leads to the question of whether older S-type main-belt families can contain Q-type objects and display evidence of a transition from Q- to S-type. To answer this question we have carried out a photometric survey of the Koronis family using the Kitt Peak 2.1m telescope. This provides a unique opportunity to compare the effects of the space weathering process on potentially ordinary chondrite-like bodies within a population of identical initial conditions. We find a trend in spectral slope for objects 1–5 km that shows the transition from Q- to S-type in the main-belt. This data set will prove crucial to our understanding of the space weathering process and its

relevant timescales.

Keywords: Asteroids; Asteroids, surfaces; Spectrophotometry

1 Introduction

Space weathering has been a long-standing puzzle in asteroid science that affects spectroscopic interpretations of near-Earth and main-belt asteroids. The biggest debate surrounding space weathering has been the potential relationship between S-type asteroids and ordinary chondrite (OC) meteorites. Visible and near-infrared spectral data have shown both similarities and discrepancies between the S-type asteroid and ordinary chondrite data sets. Although their spectra qualitatively show the same absorption features and quantitatively show evidence of the same minerals, the spectral slopes of S-type asteroid spectra are significantly reddened with respect to OC meteorites (e.g. Pieters et al. 2000, Clark et al. 2002a). For years this created great difficulties in understanding the relationship between S-type asteroids and the OC meteorites.

The line of questioning surrounding the potential influence of space weathering on asteroid surfaces mirrors discussion surrounding lunar regolith following the Apollo sample return missions. Ever since lunar soils were returned for study during the Apollo era, it has been known that mature lunar soils have the same spectral properties as telescopically obtained spectra of undisturbed surface areas (McCord et al. 1972). Yet, powdered lunar rocks and unexposed lunar regolith showed spectral differences from these surface measurements. Optical maturity causes a decrease in the band depth, increase in the spectral slope, and decrease in albedo (Adams and McCord 1971). This spectral slope mismatch has been interpreted as the result of a variety of external factors that affect constituent minerals over time, including radiation damage, solar wind implantation, and micrometeorite implantation.

The discovery of (1862) Apollo and subsequent Q-types in the near-Earth population brought to light a new spectral class that displays the best spectral match to ordinary chondrites (McFadden et al. 1985). A comparison of S- and Q-type bodies matches the idea of maturation due to space weathering on the lunar surface. Laboratory studies of maturation on the Moon implicate vapor-deposited nanophase iron as causing the observed spectral changes (Pieters et al. 2000). Quantitative modeling of maturation of ordinary chondrite spectra by adding nanophase iron is consistent with what is seen in the Q- and S-class populations (Noble et al. 2007).

Spectral changes due to space weathering should increase with time up to the point when saturation is reached and no further change occurs (e.g. Pieters et al. 2000, Noble et al. 2001). Theories on collisional evolution of small bodies show that the expected lifetime of a body varies with the asteroid size (Dohnanyi 1969, O'Brien and Greenberg 2005). A large object will have a longer collisional lifespan because it is less likely to be catastrophically disrupted. Smaller bodies will have far shorter survival times and will consequently have a younger age than their larger counterparts on average. For objects covered in regolith, the surface age need not date to the time the object was formed. Smaller impacts can seismically move regolith downslope and resurface the body (Richardson et al. 2005). Finally, the smallest objects may be unable to retain regolith due to their low surface gravity, and thus show unweathered, young-looking surfaces for very long times. Therefore, small bodies may display surfaces that are young enough to be unaltered by the space weathering process or may display surfaces that have not yet reached spectral maturity.

Current models suggest there should be a transition size below which young

surfaces should be observable. Binzel et al. (2004) identified this transition for a sample of 145 ordinary chondrite-like bodies (S-, Sq- and Q-spectral type) in near-Earth space. That study showed a trend of increasing spectral slope with increasing size over the 0.1-5 km range. The work linked ordinary chondrites to near-Earth S-type objects, but the connection to a main-belt source was incomplete. The first Q-type object was confirmed in a study of young families by Mothé-Diniz and Nesvorný (2008). That work was not able to confirm the existence of multiple fresh objects or of a transition from Q- to S-types in the main-belt. Several main belt sources have been proposed for ordinary chondrites (e.g. (6) Hebe for the H chondrites, Gaffey and Gilbert 1998), but these observations lack the final observational link between fresh ordinary chondrite-like surfaces and the current weathered objects. Finding this transition among main-belt asteroids would demonstrate a number of new conclusions: (1) that ordinary chondrites have verifiable and directly observable main-belt source regions, (2) that populations of fresh, unweathered surfaces exist in the main-belt, and (3) that near-Earth and main-belt asteroids undergo the same external processing, even if the relative strength or speed of different components may vary between the populations.

To examine the potential slope effects of space weathering in the main asteroid belt, the present work examines the spectral colors of members of the Koronis dynamical family. By studying members of a single family we intend to mitigate any differences in space weathering due to average distance from the sun. Larger members of the Koronis family have been shown to have similar S-type spectra (Barucci and Lazzarin 1993, Binzel et al. 1993), and spacecraft data from the Galileo encounter with family member (243) Ida have shown that the object is likely chondritic in composition (Chapman 1996). We assume that

these traits should extend to the small, unclassified bodies. Observing members of an undifferentiated parent body ensures that the objects share the same composition and that any observed spectral differences are due to the effects of space weathering rather than due to compositional variation within the original parent body. This provides a unique opportunity to compare the effects of the space weathering process on potentially ordinary chondrite-like bodies within a population that has essentially identical initial conditions.

This work presents the results of a photometric survey of small Koronis family members using the Kitt Peak 2.1m telescope. We performed broadband visible-wavelength spectrophotometry on 90 members of Koronis family in order to examine their spectral shape and spectral slope. First results from this project are presented in Rivkin et al. (2011). In this paper we present the details of our entire observational program (§2) and our global results (§3). In Section 4 we discuss the implications of our findings. This work completes the connection between ordinary chondrites and a potential source population in the main asteroid belt.

2 Observations and Reduction

To study the effects of space weathering within an ordinary chondritic population we need to investigate a change in slope that indicates a transition from S- to Q- taxonomic type. One approach would be to use spectroscopy, which would allow us to assign a taxonomic type to each asteroid and would provide a data set directly analogous to the Binzel et al. (2004) near-Earth asteroid investigation of the Q- to S-type transition. However, the combination of distance and small size puts our targets at magnitudes beyond the capabilities

of readily available visible and near-IR spectrographs. Instead of using traditional spectroscopy, we use broadband color photometry. This paper uses the photometry results to identify changes in average slope over a range of asteroid sizes. Using broadband colors has several advantages over attempting this survey with spectroscopy. For instance, a spectroscopic survey would require a large investment of observing time to complete. By undertaking a photometric survey we were able to use smaller telescopes (such as the 2.1-m), access larger amounts of observing time, and obtain object observations quickly and efficiently.

This study utilized the Kitt Peak 2.1-m telescope during the 2008A-2009B observing semesters. During 2008 our observations used the Harris BVRI filter set. For 2009, we sought to expand our spectrophotometry further into the near-infrared and added z filters. During 2009A we used the SDSS z' filter. Unfortunately this filter was not available for our 2009B observations and we instead used the Gunn z filter. This paper presents results from May 2008 (17 objects), December 2008-January 2009 (35 objects), April 2009 (31 objects), and September 2009 (7 objects). The objects observed, the time of observation, and the phase angle of the observation are given in Table 1. The Koronis family members observed were chosen using Stephen Slivan's online observing target calculator [1] and the Koronis family membership of Mothé-Diniz et al. (2005). Additional small targets were added using a membership list from Vokrouhlický (2006). The objects were chosen to cover a wide range of H magnitudes, which implies a wide size range. The final sample includes objects with H magnitudes from 9.24 to 16.8. All observations were taken in a sequence (e.g. VBVRVIV) that allowed us to identify and correct for lightcurve

[1] www.koronisfamily.com

variations. The correction procedure is described below.

Table 1.

All data reduction was done using the Image Reduction and Analysis Facility (IRAF). All images were calibrated using bias frames and sky flats of the appropriate filter. Most objects were observed in the north celestial hemisphere or the equatorial region of the celestial sphere. While observing in these regions we were able to use the Sloan Digital Sky Survey (SDSS) online database [2] (Abazajian et al. 2009) to identify on-frame photometric standards. We transformed the SDSS stellar magnitudes to the Johnson-Cousins photometric system using the equations presented in Jordi et al. (2006). On occasions when on-frame standards were available we were able to observe under non-photometric conditions. For each object with SDSS calibrators, at least two on-chip standards were chosen and asteroid instrumental magnitudes were calculated using differential photometry techniques. The remaining science frames required the calculation of extinction coefficients in each filter. These coefficients were calculated in the Johnson-Cousins photometric system using standard star fields from Landolt (1992) and Galadí-Enríquez et al. (2000).

Once standard-corrected asteroid magnitudes were obtained, each object was corrected for lightcurve effects. In order to quanitify the lightcurve effect, it is necessary to examine the relationships between consecutive V exposures and the exposure of the filter that the two V magnitudes have bounded. The goal is to estimate the V magnitude at the time of each exposure in the other filters. The time and magnitude change between two V exposures are defined

[2] http://cas.sdss.org/dr7/en/tools/chart/navi.asp

as Δt_V and Δm_V respectively. We define the time between a V exposure and the subsequent non-V exposure as Δt_X (where X indicates the non-V filter). To determine the value by which the V magnitude would change in time Δt_X, we define a time ratio (Δt_{VX}) that describes the time from V to X with respect to the time from V to V.

$$\Delta t_{VX} = \frac{\Delta t_X}{\Delta t_V} \tag{1}$$

This is then used to determine the change in V magnitude in the time from V to X.

$$\Delta m_{VX} = \Delta t_{VX} \times \Delta m_V \tag{2}$$

For objects in the size range observed here, we expect a rotation period greater than two hours (Warner et al. 2009). With typical exposure times of 180 seconds, the time between subsequent V exposures is extremely small compared to the minimum rotation period. Due to the small time interval between subsequent V exposures, it is assumed that the magnitude change in the minutes between V exposures is linear. This change in magnitude is used to calculate the V magnitude at the time of the X exposure. Using the concurrent V and X magnitudes, we calculate the following color indices for each object: B-V, V-R, V-I, V-z. The final V magnitude is calculated by averaging all the V magnitudes for the object. Table 2 shows the final color indices for each object.

Table 2.

The error values included in Table 2 are the result of propagation from the IRAF aperture photometry. Each individual aperture extraction (asteroid and

standard star) results in an instrumental magnitude and an error value. The instrumental errors must be convolved with the known standard star uncertainty. When on-frame standards from the SDSS online database were used, the stellar uncertainties were propagated through the Jordi et al. (2006) transformation equations and convolved with the errors of the transformation. When extinction coefficients were calculated, the errors of the individual standard star measurements were used in the linear least-squares fit. The error on the extinction coefficient was then combined with the error of the standard star and applied to the asteroid observation. All subsequent calibration calculations used standard error propagation equations.

The hypothesis for this project is that there will be a change in spectral slope and shape (from weathered S- to fresh Q-type) as a function of decreasing size. In order to test this hypothesis, we need to examine the spectral shape and spectral slope of each object in our sample. In order to conveniently compare our results to spectroscopic results, which are commonly reported in reflectance, we converted from final magnitudes and color indices to spectrophotometric reflectance values. To convert from magnitude to reflectance we need the magnitudes for each object in B, V, R, I and z and the solar colors in B-V, V-R, V-I and V-z. However, we need to be mindful of the photometric systems involved in this work. Our B, V, R and I asteroid observations were taken in the KPNO Harris filter set and calibrated using standards in the Johnson-Cousins (J-C) system. Because of this calibration by J-C system standards, we treat all final B, V, R and I asteroid magnitudes as being in the J-C photometric system. In the conversion from magnitudes to reflectances, we use the following J-C solar colors[3]: B-V=0.65, V-R=0.36, R-I 0.32. Un-

[3] http://www.sdss.org/dr6/algorithms/sdssUBVRITransform.html

fortunately, the Harris filters and the J-C filters are not exact matches in terms of wavelength coverage. Even though the asteroid magnitudes are in the J-C system, the light collected was specific to the wavelength range of the Harris filters. Due to this, we use the center wavelengths of the Harris filter set in our spectrophotometry conversion. The center wavelengths defined by Kitt Peak National Observatory [4] are λB=0.43 μm, λV=0.54 μm, λR=0.65 μm and λI=0.82 μm. Since the z filter values are available for less than half our sample they are not used in the final spectrophotometric slope calculation and therefore are not converted from magnitudes to reflectances. The z filter values on the KPNO 2.1m also suffer from limited filter transmission due to the steep drop off of the CCD efficiency curve within the z filter wavelength range. We expect that the conversion from Harris to J-C photometric colors introduces an error to our calculations that we are not able to robustly quantify. All our observations are internally consistent. However, this conversion error can affect the direct comparison of our final color indices to color indices not observed with Harris filters.

After the solar values are removed from each of the derived asteroid color indices, the object magnitudes can be converted to reflectance. The reflectance values are normalized to the V band (0.54 μm) using the following magnitude equations:

$$\left(\frac{R_X}{R_V}\right) = 10^{0.4\cdot(m_V - m_X)} = 10^{-0.4\cdot(m_X - m_V)} \tag{3}$$

where m_V and R_V are the final magnitude and reflectance of V respectively. For each filter we calculate R_X/R_V to obtain the object's normalized reflectance in that filter. This always yields a reflectance value of unity at

[4] ftp://ftp.noao.edu/kpno/filters/4Inch_List.html

0.54 μm and allows for qualitative comparison with known S-type Koronis family and Q-type near-Earth object visible reflectance spectra (which have also been normalized to unity at 0.54 μm). The errors associated with these reflectance values have been calculated from standard error propagation equations using the errors shown in Table 2.

To test the accuracy of our photometry and the magnitude to reflectance conversion we compare the spectrophotometry of our brightest objects with visible spectra from the Small Main-belt Asteroid Spectroscopic Survey (SMASS-II, Bus and Binzel 2002a). Figure 1 shows the comparison of our photometry with the SMASS spectra for three Koronis family members. Our observation of (1336) Zeelandia provides the best direct match of the three observations. In the case of (1336) Zeelandia we expect the observations to match due to their similar phase angles (α=13.4 in this work, α=15.2 in SMASS, Bus and Binzel 2002b). For the cases of (167) Urda and (720) Bohlinia we see differences in slope between the current observations and the SMASS observations, however the two asteroids are close matches to the Bus taxonomy average S spectrum (Bus and Binzel 2002a) and the spectrophotometric representation of the Dandy et al. (2003) average S color indices. We believe the mismatch of the (167) Urda observations is due to the larger phase angle of our observations (α=18.2 in this work, α=5.6 in SMASS). While the (167) Urda observation is no a direct match to the SMASS spectrum, the shape and slope of our observation is consistent with the Eight-Color Asteroid Survey (ECAS, Zellner et al. 1985). For (720) Bohlinia, the differing V-R colors are consistent with the change in phase angle (α=6.0 in this work, α=19.7 in SMASS) however this trend does not extend to the V-I color of the object in this work. We have no clear explanation for the differences between the spectrophotometry

and the SMASS spectrum for (720) Bohlinia, however we do not consider this to be detrimental to our work since the spectrophotometry closely matches the average S photometric and spectroscopic standards. For examples of Koronis family spectrophotometry consistent with Q-type spectra see Rivkin et al. (2011). To further check the accuracy of our photometry we performed a test on the (167) Urda and (720) Bohlinia frames. Since both of these objects were reduced using on frame SDSS standards, we chose two additional SDSS stars (for each object) on the frame and calculated the colors for each of these test stars. When compared to their known magnitudes, the calculated stellar colors were accurate to within a tenth of a magnitude. This demonstrates the validity of our results and puts a limit on the error due to the conversion from Harris to J-C colors.

Figure 1.

3 Results

We use calculated spectrophotometric reflectance values to examine trends in spectral slope with size for all the Koronis family members in our sample. We expect that members of a single family will have the same composition and that any slope changes seen are due to the effects of space weathering. We do not expect interlopers in our sample since the Koronis family is dynamically dense against the background population and is not expected to contain more than 1% interlopers (Zappalá et al. 1994, Milani and Farinella 1995). Furthermore, interloper asteroids in our sample can be identified from their non-S complex colors.

Theories on the collisional evolution of asteroids define the relative average surface age of asteroids (Dohnanyi 1969, O'Brien and Greenberg 2005). However, these ages are purely statistical. Any two objects of the same size may have the same collisional lifespan but will likely not have the same surface age. In order to account for this effect in our analysis of slopes we need to look at the change in average slope over average diameter.

Figure 2.

Figure 2 shows the slope versus H magnitude (bottom axis) and approximate object diameter (top axis) for all the Koronis family objects in our sample. Black circles show the spectrophotometric slope for each individual object in the sample. Object slopes were calculated using a least squares fit through the four spectrophotometric reflectance points at the B, V, R and I wavelengths (0.43–0.82 μm). The error for each object's slope was found via a Monte Carlo calculation. The spectrophotometric values were altered by applying an offset equal to the calculated error value convolved with a random number (gaussian distribution from -1 to 1). This process was repeated ten thousand times for each object with a new slope being calculated for each instance of this spectrum. The error is then calculated as the standard deviation of the slopes generated by this process. Object diameter was determined using the H magnitudes provided for the objects by the Minor Planet Center. Although catalog H magnitudes can have errors of $\sim$0.5 mag (Jurić et al. 2002, Romanishin and Tegler 2005), those errors may be systematic and would not affect the overall trend presented here. The conversion from H magnitude to diameter was calculated using Eq. 2 of Harris and Harris (1997), assuming a constant S-type albedo of 0.239 (Stuart and Binzel 2004). Even though the results presented here and in Rivkin et al. (2011) suggest that there are Q-type objects present

in our sample, we use a constant albedo for all objects in our sample. Using a higher albedo for Q-like objects would reduce their sizes and thus increase the trend shown in Figure 2.

The two parallel lines indicate the slope values for the average S- and Q-type reflectances calculated from the color indices presented in Dandy et al. (2003). The red squares show a running box mean (bin size=35). The bin size was chosen to display the average of large subsections of the population while remaining significantly lower than a majority of the population. It is comparable to the bin size chosen (50 for 145 targets) by Binzel et al. (2004). The error for each average slope value is simply the propagation of each individual slope error.

We find a clear change in the average slope from the smallest to the largest asteroids in our sample. The running box mean displays the full range of slopes in the transition from the average Q-type to the average S-type value. The apparent discontinuity at 5 km is a consequence of the sorting algorithms ordering of objects with equivalent H magnitudes and has no physical interpretation. The trend from Q- to S-type slopes is independent of sorting.

The running box mean trend shown in Fig. 2 displays a steep slope from the small size limit of the observational sample until an average diameter of approximately 5 km is reached. At this diameter the running box trend drastically changes slope and slowly approaches the average S-type value. This two sloped space weathering trend matches the trend presented in Vernazza et al. (2009). The work by Vernazza et al. suggests that the steep slope at smaller sizes is the result of rapid weathering via the solar wind ion implantation process and is followed by a longer timescale weathering (shallower slope,

larger sizes) due to micrometeorite impacts. This work is the first to show this two-pronged weathering process within a single family.

Figure 3a and 3b.

In order to further illustrate existence of an S- to Q- type transition in the Koronis family, we also compare the color indices of the objects with typical values for the Q and S taxonomic classes (Dandy et al. 2003). Figure 3a shows V-I versus V-R for all objects in our dataset and shows the range of objects with respect to the Dandy class averages. Figure 3b shows the S- and Q-type averages with a contour plot of the V-I versus V-R values. The contours start at the center of the color index distribution and proceed outward with a contour around each successive 10 objects. These figures show that the center of the data distribution is between the S- and Q-type averages and that most objects display colors filling the color transition space between the two type averages and surrounding the S- and Q-type averages. Most outliers are observations with large error bars.

4 Discussion

Our conclusions assume that the change in spectral slope demonstrated by the Koronis family observations is due to space weathering. There are other physical and observational effects that influence spectral slope that can be ruled out for this dataset. An important factor to consider is the effect of phase angle on the asteroid observations. Laboratory measurements of meteorites and telescopic observations of asteroids have shown that spectral slopes increase with increasing phase angle (e.g. Bowell and Lumme 1979, Clark et al. 2002b,

Nathues 2010). The phase angles of each of our object observations have been included in Table 1. All objects were observed at a phase angle less than ∼21 degrees and the observed slopes show no dependence on phase angle. Another factor to consider is the metal content of an object. It has been demonstrated that increased metal content in silicate-metal mixtures can increase the spectral slope (e.g. Cloutis et al. 1986). While we cannot definitively decouple the effects of metal and space weathering on our observations, we find it unlikely that our trend is due to changes in metal content within our sample. The Koronis family was chosen in order to minimize compositional effects. We expect a fairly consistent composition across the family and previous work strongly suggests the objects are ordinary chondritic. There is no evidence to suggest that there would be a trend of increasing metal content with increasing size within this family.

This work assumes lunar-style space weathering occurs within the Koronis family. However, spacecraft missions have shown that not all asteroids follow the well understood lunar-style weathering process. In assuming lunar-style weathering, we expect that over time the spectral slope increases, band depth decreases, and albedo decreases (e.g. Pieters et al. 2000, Noble et al. 2001). NEAR observations of Eros show the space weathering process to consist of decreases in albedo, subtle decreases in band depth (Murchie et al. 2002), and no change in slope (Bell et al. 2002). However, on the Koronis family member Ida, Galileo observations show the space weathering process to produce minimal change in albedo (Veverka et al. 1996) with clear decreases in band depth and increases in slope (Helfenstein et al. 1996). A more thorough examination of the different space weathering styles are presented in Gaffey (2010). If the space weathering process occurring in the Koronis family is not lunar-style,

then we expect Ida-style weathering to occur. Our primary result of increasing average slope with increasing average object size and therefore increasing average age is compatible with the Ida-style weathering process. Neither this paper nor Rivkin et al. (2011) investigate the albedo changes within the family. We defer this discussion to a forthcoming paper by our group presenting albedos for small Koronis family members (Trilling et al., in prep).

For objects smaller than 5 km the average slopes suggest that the objects have fresh or partially weathered surfaces. While this information alone does not provide insight into the timescales of space weathering or the processes counteracting it, our results are consistent with previously published timelines. Nesvorný et al. (2010) finds that Q-type spectra persist for at least 1 Myr on main-belt objects, while Willman et al. (2010) find the space weathering process nears completion in a period of 960 Myr. Our findings are consistent with the Nesvorný et al. (2010) and the Willman et al. (2010) timescales when one considers the processes acting toward the freshening of surfaces. The simulations presented in O'Brien and Greenberg (2005) show that an object approximately 5 km in diameter will have a main-belt collisional lifetime of approximately 1000 Myr. Catastrophic disruptions on these intervals would cause a small population of not fully space weathered bodies in the Koronis family. In addition to the creation of fresh surfaces via catastrophic collisions, smaller collisions on a body covered in regolith can cause regolith movement capable of resetting the surface age (Richardson et al. 2005). The average time interval for an impact to destabilize the surface but not catastrophically disrupt a 5 km body can be as small as $\sim 10^2 - 10^3$ years. It is likely that the fresh and partially weathered surfaces present in the Koronis family are due to a combination of both smaller, more frequent collisions resetting the surface

regolith on regional scales and large catastrophic collisions. The work of Binzel et al. (2010) states that planetary encounters are the primary mechanism for freshening surfaces in the near-Earth population. Our survey of the main-belt Koronis family shows that in the absence of planetary encounters, collisional processes are sufficient to freshen weathered S-type surfaces.

The running box mean in Figure 2 shows a steep slope from the small size limit of the sample until an average diameter of $\sim$5 km, where the slope changes drastically. The trend presented for the Q- to S- type transition in near-Earth space follows this same two slope structure (Binzel et al. 2004). We note that the change in slope for both the Koronis family and near-Earth space occurs at approximately 5 km. Due to higher collisional rates in the main-belt, we do not expect 5 km bodies in near-Earth space and in the main-belt to have the same average surface ages, collisional lifetimes, or periods between resurfacing events. We do not expect space weathering to act on the same timescales in both asteroid regions. (Nesvorný et al. (2010) states that the solar wind component of the space weathering timescale goes as q^2.) Perhaps it is the case that the processes acting toward (solar wind, micrometeorites) and against (collisions, planetary encounters) space weathering have coincidentally balanced in such a manner as to approach space weathering saturation at a diameter of 5 km in both near-Earth space and in the Koronis family.

Many authors (e.g. Gaffey et al. 1993, Hiroi et al. 1993) have shown that the S taxonomic class is composed of several distinct compositional subclasses comprised of bodies such as ordinary chondrites, primitive achondrites, and stony iron meteorites. For the Koronis family we have spacecraft data from the Galileo encounter with family member (243) Ida that point toward a chondritic nature for the body (Chapman 1996). Surveys like this present work can be

used to compare the space weathering rate of ordinary chondrite-like bodies to that of families of different taxonomic type or different S-type composition in the main-belt.

It is possible that future spectrophotometric surveys will not require slope to probe the transition from Q- to S-type bodies. Another method of probing the space weathering transition is to examine the band depth due to olivine and/or pyroxene. This cannot be done using BVRI filters, but is possible with Sloan filters. The Sloan i' center wavelength (0.763 μm) covers the spectral peak while the Sloan z' center wavelength (0.913 μm) is deep within the absorption feature. These color indices would measure the downward slope into the 1-μm olivine and pyroxene absorption feature. By examining the change of these color indices with size, one could investigate the transition from Q- to S-type body. This procedure could be relevant to the Sloan filter data from large upcoming surveys such as Pan-STARRS [5] and the Large Synoptic Survey Telescope [6].

5 Conclusions

We present the first results to examine space weathering within a large, old asteroid family. By observing members of an ordinary chondritic family we ensure that all objects share the same initial composition and that any changes in spectrophotometric slope and shape are due to space weathering. We have identified a trend of increasing spectral slope with increasing size that displays the transition from Q- to S-type bodies in the Koronis family for bodies in

[5] http://pan-starrs.ifa.hawaii.edu/

[6] http://www.lsst.org/

the 1–5 km range. The steep trend in spectral slope from the smallest asteroid size to 5 km shows that on average family members in this size range display surfaces that are not fully space weathered. This trend spans slopes from average Q-type to average S-type. This suggests that a number of fresh, Q-type bodies are present in our sample and in the family as a whole. An investigation of the observed color indices supports our conclusion that a transition from Q- to S-type colors exists in our sample. The identification of fresh surfaces in the main-belt shows that planetary encounters are not necessary for the existence of fresh, Q-type surfaces.

Acknowledgements

The authors would like to thank Di Harmer, Bill Binkert, and John Glaspey for their assistance obtaining and calibrating the Harris filter transmission curves. We also thank Steve Tegler for many conversations about broadband photometry and Rick Binzel for discussions concerning space weathering. CAT was supported in part by the National Science Foundation Graduate Research Fellowship program. ASR was supported by NSF Planetary Astronomy grant 0708101. This work was also supported by funding from the Spitzer Space Center/JPL.

References

Abazajian, K.N, et al. 2009. The Seventh Data Release of the Sloan Digital Sky Survey. The Astrophysical Journal Supplement Series 182, 543-558.

Adams, J.B., McCord, T.B., 1971. Alteration of lunar optical properties: age and composition effects. Science 171, 567-571.

Barucci, M.A., Lazzarin, M., 1993. Koronis family: reflectance spectra of 243 Ida, 1442 Corvina and 2226 Cunitza. Planetary and Space Science 41, 641-646.

Bell III, J.F., Izenberg, N.I., Lucey, P.G., Clark, B.E., Peterson, C., Gaffey, M.J., Joseph, J., Carcich, B., Harch, A., Bell, M.E., Warren, J., Martin, P.D., McFadden, L.A., Wellnitz, D., Murchie, S., Winter, M., Veverka, J., Thomas, P., Robinson, M.S., Malin, M., Cheng, A., 2002. Near-IR Reflectance Spectroscopy of 433 Eros from the NIS Instrument on the NEAR Mission: I. Low Phase Angle Observations. Icarus 155, 119-144.

Binzel, R.P., Xu, S., Bus, S.J., 1993. Spectral Variations within the Koronis Family: Possible Implications for the Surface Colors of Asteroid 243 Ida. Icarus 106, 608-611

Binzel, R.P., Rivkin, A.S., Stuart, J.S., Harris, A.W., Bus, S.J., Burbine, T.H., 2004. Observed Spectral Properties of near-Earth objects: Results for Population Distribution, Source Regions, and Space Weathering Processes. Icarus 170, 259-294.

Binzel, R. P., Morbidelli, A., Merouane, S., DeMeo, F. E., Birlan, M., Vernazza, P., Thomas, C. A., Rivkin, A. S., Bus, S. J., and Tokunaga, A. T., 2010. Earth encounters as the origin of fresh surfaces on near-Earth asteroids.

Nature 463, 331-334.

Bowell, E., Lumme, K., 1979. Colorimetry and magnitudes of asteroids. In: Gehreis, T. (Ed.), Asteroids, University of Arizona Press, Tucson, pp. 132-139.

Bus, S.J., Binzel, R.P., 2002a. Phase II of the Small Main-Belt Asteroid Spectroscopic Survey: A Feature-Based Taxonomy. Icarus 158, 146-177.

Bus, S.J., Binzel, R.P., 2002b. Phase II of the Small Main-Belt Asteroid Spectroscopic Survey: The Observations. Icarus 158, 106-145.

Chapman, C.R., 1996. S-type asteroids, ordinary chondrites, and space weathering: The evidence from Galileos fly-bys of Gaspra and Ida. Meteoritics and Planetary Science 31, 699-725.

Clark, B. E., Hapke, B., Pieters, C., and Britt, D., 2002a. Asteroid space weathering and regolith evolution. In: Bottke, W., Cellino, A., Paolicchi, P., and Binzel, R. P. (Eds.), Asteroids III, University of Arizona Press, Tucson, pp. 585-599.

Clark, B. E., Helfenstein, P., Bell III, J.F., Peterson, C., Veverka, J., Izenberg, N.I., Domingue, D., Wellnitz, D., McFadden, L., 2002b. NEAR infrared spectrometer photometry of Asteroid 433 Eros. Icarus 155, 189-204.

Cloutis, E.A., Gaffey, M.J., Jackowski, T.L., Reed, K.L., 1986. Calibrations of phase abundance, composition, and particle size distribution for olivine-orthopyroxene mixtures from reflectance spectra. J. Geophys. Res. 91, 11641-11653.

Dandy, C.L., Fitzsimmons, A., and Collander-Brown, S.J. 2003. Optical colors of 56 near-Earth objects: trends with size and orbit. Icarus 163, 363-373.

Dohnanyi, J.S., 1969. Collisional Model of Asteroids and Their Debris. Journal of Geophysical Research 74, 2531-2554.

Gaffey, M. J., Bell, J.F., Brown, R.H., Burbine, T.H., Piatek, J.L., Reed, K.L, Chaky, D.A., 1993. Mineralogical variations within the S-type asteroid class. Icarus 106, 573-602.

Gaffey, M.J., Gilbert, S.L., 1998. Asteroid 6 Hebe: The probable parent body of the H-type ordinary chondrites and the IIE iron meteorites. Meteoritics and Planetary Science 33, 1281-1295.

Gaffey, M.J., 2010. Space weathering and the interpretation of asteroid reflectance spectra. Icarus 209, 564-574.

Galadí-Enríquez, D., Trullols, E., Jordi, C., 2000. Secondary UBVRI-CCD standard stars in the neighborhood of Landolt standard stars. Astronomy and Astrophysics Supplement Series 146, 169-177.

Harris, A.W. and Harris, A.W. 1997. On the Revision of Radiometric Albedos and Diameters of Asteroids. Icarus 126, 450-454.

Helfenstein, P., Veverka, J., Thomas, P.C., Simonelli, D.P., Klaasen, K., Johnson, T.V., Fanale, F., Granahan, J., McEwen, A.S., Belton, M., Chapman, C., 1996. Galileo Photometry of Asteroid 243 Ida. Icarus 120, 48-65.

Hiroi, T., Bell, J.F., Takeda, H., Pieters, C.M. 1993. Modeling of S-type asteroid spectra using primitive achondrites and iron meteorites. Icarus 102, 107-116.

Jordi, K., Grebel, E.K., and Ammon, K. 2006. Empirical color transformations between SDSS photometry and other photometric systems. Astronomy and

Astrophysics 460, 339-347.

Jurić, M., Ivezić, Ẑ, Lupton, R.H, Quinn, T., Tabachnik, S., Fan, X., Gunn, J.E., Hennessy, G.S., Knapp, G.R., Munn, J.A., Pier, J.R., Rockosi, C.M, Schneider, D.P., Brinkmann, J., Csabai, I.,and Fukugita, M., 2002. Comparison of positions and magnitudes of asteroids observed in the Sloan Digital Sky Survey with those predicted for known asteroids. The Astronomical Journal 124, 1776-1787.

Landolt, A.U., 1992. UBVRI Photometric Standard Stars in the Magntiude Range 11.5 $<$ V $<$ 16.0 Around the Celestial Equator. The Astronomical Journal 104, 340-371.

McCord, T.B., Charette, M.P., Johnson, T.V., Lebofsky, L.A., Pieters, C. 1972. Spectrophotometry (0.3 to 1.1μm) of visited and proposed apollo lunar landing sites. The Moon, 5, 52-89.

McFadden, L.A., Gaffey, M.J., McCord, T.B., 1985. Near-Earth Asteroids: Possible Sources from Reflectance Spectroscopy. Science 229, 160-163.

Milani, A. and Farinella, P. 1995. An Asteroid on the Brink. Icarus 115, 209-212.

Mothé-Diniz, T., Roig, F., and Carvano, J.M., 2005. Mothe-Diniz Asteroid Dynamical Families. EAR-A-VARGBDET-5-MOTHEFAM-V1.0. NASA Planetary Data System.

Mothé-Diniz, T., Nesvorny, D., 2008. Visible spectroscopy of extremely young asteroid families. Astronomy & Astrophysics 486, L9-L12.

Murchie, S., Robinson, M., Clark, B., Li, H., Thomas, P., Joseph, J., Bussey,

B., Domingue, D., Veverka, J.,, Izenberg, N., Chapman, C., 1996. Color Variations on Eros from NEAR Multispectral Imaging. Icarus 155, 145-168.

Nathues, A., 2010. Spectral study of the Eunomia asteroid family Part II: The small bodies. Icarus 208, 252-275.

Nesvorný, D., Bottke, W.F., Vokrouhlický, D., Chapman, C.R., Rafkin, S., 2010. Do planetary encounters reset surfaces of Near Earth Asteroids? Icarus 209, 510-519.

Noble, S.K., Pieters, C.M., Taylor, L.A., Morris, R.V., Allen, C.C., McKay, D.S. and Keller, L.P., 2001. The optical properties of the finest fraction of lunar soil: Implications for space weathering, Meteorit. Planet. Sci. 36, 31-42.

Noble, S.K., Pieters, C.M., Keller, L.P., 2007. An experimental approach to understanding the optical effects of space weathering. Icarus 192, 629-642.

O'Brien, D.P., Greenberg, R., 2005. The collisional and dynamical evolution of the main-belt and NEA size distributions. Icarus 178, 179-212.

Pieters, C.M., Taylor, L.A., Noble, S.K., Keller, L.P., Hapke, B., Morris, R.V., Allen, C.C., McKay, D.S., Wentworth, S., 2000. Space Weathering on Airless Bodies: Resolving a Mystery with Lunar Samples. Meteoritics and Planetary Science 35, 1101-1107.

Richardson, J. E., Melosh, H. J., Greenberg, R. J., OBrien, D. P. 2005. The global effects of impact-induced seismic activity on fractured asteroid surface morphology. Icarus 179, 325-349.

Rivkin, A.S, Thomas, C.A., Trilling, D.E., Enga, M., Grier, J.A., 2011. Ordinary Chondrite-colors in small Koronis Family members. Icarus, in press.

Romanishin, W., Tegler, S.C., 2005. Accurate absolute magnitudes for Kuiper belt objects and Centaurs. Icarus 179, 523-526.

Stuart, J.S., and Binzel, R.P. 2004. Bias-corrected population, size-distribution and impact hazard for the near-Earth objects. Icarus 170, 295-311.

Vernazza, P., Binzel, R.P., Rossi, A., Fulchignoni, M., Birlan, M., 2009. Solar wind as the origin of rapid reddening of asteroid surfaces. Nature 458, 993-995.

Veverka, J., Helfenstein, P., Lee, P., Thomas, P., McEwen, A., Belton, M., Klaasen, K., Johnson, T.V., Granahan, J., Fanale, F., Geissler, P., Head III, J.W., 1996. Ida and Dactyl: Spectral Reflectance and Color Variations. Icarus 120, 66-76.

Vokrouhlický, D., 2006. personal communication.

Warner, B.D., Harris, A.W., Pravec, P., 2009. The asteroid lightcurve database. Icarus 202, 134-146.

Willman, M., Jedicke, R., Moskovitz, N., Nesvorný, D., Vokroulický, D., Mothé-Diniz, T., 2010. Using the youngest asteroid clusters to constrain the space weathering and gardening rate on S-complex asteroids. Icarus 208, 758-772.

Zappalá, V., Cellino, A., Farinella, P., and Milani, A. 1994. Asteroid families, II. Extension to unnumbered multiopposition asteroids. Astronomical Journal 107, 772-801.

Zellner, B., Tholen, D.J., Tedesco, E.F., 1985. The Eight Color Asteroid Survey: Results for 589 Minor Planets. Icarus 61, 355-416.

Table 1. Table of Observations. The table contains asteroid name and number, date and time UT, and phase angle.

Table 2. Asteroid Results. The table lists the asteroid name and number, the observed color indices with their corresponding error values, and the calculated slope and slope error. When available, the V- z' or V - Gunn z value is included. The associated V-z error corresponds to either the V-z' or V-Gunn z magnitude, whichever (if either) is present.

Figure 1. Spectrophotometric results from this survey for (167) Urda, (720) Bohlinia, and (1336) Zeelandia compared to spectra of the objects from the Small Main-Belt Asteroid Spectroscopic Survey (SMASS-II, Bus and Binzel 2002a). These three objects are the only overlap between SMASS and our survey. The small overlap is due to our survey's focus on smaller objects. The data for (1336) Zeelandia show the best match of the three asteroids. Even though the data for (167) Urda and (720) Bohlinia do not fully match their corresponding SMASS spectrum, we are confident in our data since they are within the range expected for S-type objects

Figure 2. Slope vs. H magnitude and approximate object diameter for all the objects in the Koronis family dataset. Black circles show the spectrophotometric slope for each of the individual objects in the sample. The slopes were calculated using a least-squares fit to reflectance values at the calculated B, V, R, and I Harris filter wavelengths. H magnitude is shown along the bottom axis with its corresponding object diameter shown on the top axis. The conversion from H magnitude to diameter was calculated using Eq. 2 of Harris and Harris (1997) and assuming a constant S-type object albedo of 0.239 (Stuart and Binzel 2004). The two parallel lines indicate the slope values for the average S-

and Q-type reflectances calculated from the color indices presented in Dandy et al. (2003). The red squares show a running box mean (box size=35). We find a clear change in average slope from the smallest to the largest asteroids in our sample. The running box mean trend shows a steep slope from the small size limit of the observational sample until an average diameter of approximately 5 km is reached. At this diameter the running box trend drastically changes slope and slowly approaches the average S-type value. The change in slope of this running box trend at 5 km is the same upper limit of the spectral trend found in the near-Earth population (Binzel et al. 2004).

Figure 3. (a) Color indices V-I vs. V-R for all objects in the Koronis dataset plotted with the average S- and Q-type colors from Dandy et al. (2003). (b) The contours display the distribution of objects surrounding the center of the V-I vs. V-R cluster. The contours start at the center of the color index distribution and proceed outward with a contour around each successive 10 objects. The figures illustrate the distribution of objects with respect to the S- and Q- type averages. We find that the center of the distribution is between the S- and Q- type averages and that most objects reside in the space between and surrounding the two type averages.

Table 1: Observations

Number	Name	UT Date	UT Time	Phase Angle
17082	1999 JC3	3 May 2008	5:13 - 5:56	17.4
250694	2005 QX 122	4 May 2008	5:14 - 6:42	12.3
7597	Shigemi	4 May 2008	6:52 - 7:35	9.6
187223	2005 SX139	5 May 2008	3:48 - 4:58	12.1
17107	1999 JJ51	6 May 2008	3:32 - 4:19	19.0
18462	Ricco	6 May 2008	4:26 - 5:04	16.3
19017	Susanlederer	6 May 2008	5:22 - 6:09	12.6
21137	1993 FX20	6 May 2008	6:14 - 7:01	11.0
32323	2000 QW60	6 May 2008	7:30 - 8:15	12.6
46321	2001 QO84	7 May 2008	3:40 - 4:21	19.3
37361	2001 UW46	7 May 2008	4:27 - 5:08	20.2
37411	2001 XH152	7 May 2008	5:20 - 5:58	13.6
36609	2000 QD144	7 May 2008	6:07 - 7:04	11.0
35251	1995 YE5	7 May 2008	7:12 - 8:10	11.8
35555	1998 FC120	8 May 2008	4:57 - 6:13	13.7

Number	Name	UT Date	UT Time	Phase Angle
36600	2000 QP138	8 May 2008	6:20 - 6:57	14.2
36518	2000 QC77	8 May 2008	7:08 - 7:46	14.4
9908	Aue	31 Dec 2008	2:17 - 3:00	19.9
26334	1998 WD15	31 Dec 2008	3:20 - 4:02	15.8
14256	2000 AA96	31 Dec 2008	4:17 - 4:53	13.3
27449	2000 GD14	31 Dec 2008	6:15 - 7:28	2.1
27364	2000 EJ14	31 Dec 2008	7:53 - 8:25	5.8
30563	2001 OZ75	31 Dec 2008	8:33 - 9:15	5.5
28221	1998 YG17	31 Dec 2008	9:33 - 10:15	11.0
28665	2000 GN51	31 Dec 2008	10:22 - 11:09	13.2
28747	2000 GF151	31 Dec 2008	11:28 - 12:14	15.7
1079	Mimosa	1 Jan 2009	2:44 - 3:04	20.2
25106	Ryoojungmin	1 Jan 2009	3:23 - 4:01	18.3
9757	Felixdejager	1 Jan 2009	4:07 - 5:00	13.1
6284	Borisivanov	1 Jan 2009	5:20 - 6:11	6.1

Number	Name	UT Date	UT Time	Phase Angle
29050	3333 T-2	1 Jan 2009	6:36 - 7:42	1.1
14281	2000 CR92	1 Jan 2009	8:03 - 8:46	7.4
45508	2000 BN18	2 Jan 2009	5:53 - 6:29	14.1
45695	2000 ET150	2 Jan 2009	6:34 - 7:26	5.2
13382	1998 XC4	2 Jan 2009	8:36 - 9:06	8.3
30286	2000 HG61	2 Jan 2009	9:23 - 10:09	10.9
27963	1997 ST2	2 Jan 2009	10:14 - 11:16	18.4
7260	Metelli	2 Jan 2009	11:35 - 12:09	20.1
28833	2000 JB35	2 Jan 2009	12:15 - 12:50	19.9
13112	Montmorency	3 Jan 2009	2:26 - 3:35	19.2
46193	2001 FW141	3 Jan 2009	3:59 - 4:34	14.3
45654	2000 EV71	3 Jan 2009	4:40 - 5:21	13.0
658	Asteria	3 Jan 2009	5:30 - 5:48	6.9
43996	1997 QH	3 Jan 2009	6:49 - 7:25	2.9
45610	2000 DJ48	3 Jan 2009	7:35 - 8:12	1.2

Number	Name	UT Date	UT Time	Phase Angle
14797	1977 XZ2	3 Jan 2009	8:18 - 8:53	6.9
28707	2000 GZ94	3 Jan 2009	9:09 - 9:44	12.6
27502	Stephbecca	3 Jan 2009	9:49 - 10:24	14.7
14443	1992 TV	3 Jan 2009	10:29 - 11:03	14.1
26970	Elias	3 Jan 2009	11:19 - 11:54	18.0
34720	2001 PH54	3 Jan 2009	12:01 - 12:36	20.0
24750	Ohm	3 Jan 2009	12:40 - 13:25	19.8
27448	2000 GQ6	2 April 2009	3:23 - 4:14	16.7
1336	Zeelandia	2 April 2009	4:28 - 4:58	13.4
30172	2000 GZ71	2 April 2009	5:02 - 5:51	12.3
26873	1994 AP7	2 April 2009	5:56 - 6:45	11.2
15281	1991 PT16	2 April 2009	6:53 - 7:43	7.8
15277	1991 PC7	2 April 2009	7:48 - 8:38	5.0
3726	Johnadams	3 April 2009	4:24 - 5:12	15.0
30254	2000 HZ25	3 April 2009	5:17 - 6:08	15.8

Number	Name	UT Date	UT Time	Phase Angle
15277	1991 PC7	3 April 2009	8:47 - 9:36	5.4
5523	Luminet	3 April 2009	10:00 - 10:46	6.4
16313	1199 T-1	4 April 2009	3:41 - 4:32	12.9
39684	1996 PD8	4 April 2009	4:48 - 5:46	12.5
28853	2000 JX55	4 April 2009	6:10 - 7:00	13.4
16254	Harper	4 April 2009	7:05 - 7:49	6.6
28341	Bingaman	4 April 2009	7:54 - 8:42	4.4
28342	1999 FB9	5 April 2009	5:00 - 5:49	9.5
16249	Cauchy	5 April 2009	7:15 - 8:10	4.9
8102	Yoshikazu	5 April 2009	8:15 - 9:16	3.7
29211	1991 RY15	5 April 2009	9:20 - 10:08	1.6
2092	Sumiana	6 April 2009	3:22 - 4:13	19.6
167	Urda	6 April 2009	5:23 - 5:45	18.2
3032	Evans	6 April 2009	5:53 - 6:25	2.3
5918	1991 NV3	6 April 2009	6:30 - 7:01	2.2

Number	Name	UT Date	UT Time	Phase Angle
30305	Severi	6 April 2009	7:04 - 8:07	2.1
15573	2000 GX65	7 April 2009	2:45 - 3:48	17.8
2144	Marietta	7 April 2009	3:52 - 4:37	19.3
28028	1998 DS8	7 April 2009	4:41 - 5:36	18.9
15578	2000 GW69	7 April 2009	5:41 - 6:34	16.0
5583	Braunerova	7 April 2009	6:42 - 7:10	2.1
5882	1992 WW5	7 April 2009	7:13 - 7:56	3.2
16014	Sinha	7 April 2009	8:01 - 9:01	4.1
720	Bohlinia	9 Sept 2009	9:17 - 10:10	6.0
6820	Buil	9 Sept 2009	10:17 - 11:19	20.5
17779	Migomueller	10 Sept 2009	4:24 - 5:15	14.7
35249	1995 WQ3	10 Sept 2009	5:58 - 6:47	7.6
20584	Brigidsavage	10 Sept 2009	7:22 - 8:12	2.1
39145	2000 WU90	10 Sept 2009	8:40 - 9:30	8.2
23050	1999 XJ36	15 Sept 2009	10:35 - 11:23	21.1

Table 2: Asteroid Results

Number	Name	H	D(km)	B-V	σ_{B-V}	V-R	σ_{V-R}	V-I	σ_{V-I}	V-z'	V-Gunn z	σ_{V-z}	Slope	σ_{Slope}
167	Urda	9.24	38.6	0.920	0.016	0.459	0.017	0.870	0.010	0.443		0.014	1.01	0.04
658	Asteria	10.54	21.2	0.847	0.008	0.452	0.008	0.836	0.009				0.79	0.03
720	Bohlinia	9.71	31.1	0.771	0.008	0.404	0.006	0.834	0.006		0.411	0.007	0.64	0.02
1079	Mimosa	11.20	15.6	0.887	0.008	0.478	0.009	0.855	0.009				0.92	0.03
1336	Zeelandia	10.66	20.1	0.935	0.017	0.431	0.021	0.827	0.014	0.412		0.016	0.90	0.05
2092	Sumiana	11.8	11.9	1.205	0.045	0.571	0.038	0.976	0.017	0.643		0.045	1.77	0.09
2144	Marietta	11.0	17.2	0.827	0.011	0.464	0.012	0.938	0.008	0.450		0.011	1.05	0.03
3032	Evans	11.4	14.3	0.694	0.026	0.564	0.044	0.803	0.014	0.380		0.009	0.49	0.07

Number	Name	H	D(km)	B-V	σ_{B-V}	V-R	σ_{V-R}	V-I	σ_{V-I}	V-z'	V-Gunn z	σ_{V-z}	Slope	σ_{Slope}
3726	Johnadams	12.0	10.8	0.912	0.036	0.380	0.028	0.804	0.023	0.524		0.033	0.78	0.09
5523	Luminet	12.7	9.9	0.883	0.024	0.397	0.025	0.866	0.022	0.684		0.048	0.91	0.08
5583	Braunerova	12.4	9.0	0.792	0.010	0.480	0.010	0.829	0.008	0.442		0.010	0.69	0.03
5882	1992 WW5	13.8	4.7	0.569	0.078	0.366	0.055	0.815	0.061	0.465		0.048	0.17	0.25
5918	1991 NV3	12.8	7.5	0.817	0.046	0.422	0.030	0.841	0.025	0.449		0.026	0.74	0.12
6284	Borisivanov	13.0	6.8	0.856	0.008	0.460	0.009	0.875	0.014				0.92	0.04
6820	Buil	12.5	8.6	1.059	0.064	0.407	0.042	0.919	0.038		0.550	0.043	1.32	0.16
7260	Metelli	13.0	6.8	0.928	0.024	0.421	0.057	0.751	0.054				0.69	0.14

Number	Name	H	D(km)	B-V	σ_{B-V}	V-R	σ_{V-R}	V-I	σ_{V-I}	V-z'	V-Gunn z	σ_{V-z}	Slope	σ_{Slope}
7597	Shigemi	12.6	8.2	0.852	0.008	0.445	0.007	0.810	0.007				0.73	0.02
8102	Yoshikazu	13.3	5.9	0.753	0.058	0.464	0.052	0.926	0.077	0.515		0.037	0.89	0.26
9757	Felixdejager	13.2	6.2	0.861	0.010	0.436	0.007	0.766	0.008				0.63	0.03
9908	Aue	13.2	6.2	0.863	0.010	0.459	0.009	0.859	0.012				0.88	0.04
13112	Montmorency	13.8	4.7	0.899	0.022	0.436	0.018	0.763	0.016				0.68	0.05
13382	1998 XC4	12.9	7.2	0.846	0.011	0.457	0.008	0.859	0.009				0.86	0.03
14256	2000 AA96	13.1	6.5	0.863	0.009	0.438	0.009	0.824	0.009				0.78	0.03
14281	2000 CR92	13.1	6.5	0.861	0.009	0.465	0.009	0.842	0.009				0.84	0.03

Number	Name	H	D(km)	B-V	σ_{B-V}	V-R	σ_{V-R}	V-I	σ_{V-I}	V-z'	V-Gunn z	σ_{V-z}	Slope	σ_{Slope}
14443	1992 TV	13.2	6.2	0.924	0.012	0.494	0.009	0.961	0.011				1.29	0.04
14797	1977 XZ2	13.2	6.2	0.840	0.012	0.457	0.008	0.844	0.010				0.81	0.03
15277	1991 PC7	13.4	5.7	0.993	0.079	0.407	0.067	1.008	0.059	0.121		0.106	1.73	0.30
15277	1991 PC7	13.4	5.7	1.111	0.127	0.388	0.107	1.098	0.152	1.654		0.274	1.73	0.30
15281	1991 PT16	13.0	6.8	0.935	0.114	0.468	0.061	0.926	0.064	1.130		0.091	1.19	0.28
15573	2000 GX65	13.7	4.9	0.753	0.075	0.466	0.091	0.942	0.071	0.259		0.074	0.93	0.27
15578	2000 GW69	13.4	5.7	0.971	0.097	0.426	0.050	0.838	0.059	0.366		0.062	0.98	0.24
16014	Sinha	13.9	4.5	1.040	0.056	0.478	0.038	0.711	0.129				0.78	0.32

Number	Name	H	D(km)	B-V	σ_{B-V}	V-R	σ_{V-R}	V-I	σ_{V-I}	V-z'	V-Gunn z	σ_{V-z}	Slope	σ_{Slope}
16249	Cauchy	14.8	3.0	1.185	0.102	0.313	0.055	0.603	0.056	0.229		0.069	0.65	0.21
16254	Harper	14.6	3.3	0.672	0.105	0.336	0.078	0.920	0.084	0.503		0.071	0.66	0.34
16313	1199 T-1	14.2	3.3	1.107	0.371	0.303	0.140	0.760	0.126	1.414		0.139	0.91	0.71
17082	1999 JC3	13.1	6.5	0.878	0.015	0.427	0.029	0.788	0.017				0.71	0.05
17107	1999 JJ51	13.1	6.5	0.841	0.034	0.438	0.031	0.770	0.028				0.60	0.09
17779	Migomueller	13.8	4.7	1.230	0.022	0.489	0.016	0.890	0.021				1.50	0.07
18462	Ricco	14.7	3.1	0.801	0.069	0.425	0.055	0.464	0.057				-0.14	0.16
19017	Susanlederer	15.0	2.7	0.914	0.036	0.278	0.041	0.593	0.037				0.24	0.10

Number	Name	H	D(km)	B-V	σ_{B-V}	V-R	σ_{V-R}	V-I	σ_{V-I}	V-z'	V-Gunn z	σ_{V-z}	Slope	σ_{Slope}
20584	Brigidsavage	14.8	3.0	0.933	0.089	0.386	0.039	0.854	0.033		0.239	0.051	0.95	0.19
21137	1993 FX20	14.0	4.3	0.863	0.028	0.498	0.031	0.795	0.033				0.73	0.10
23050	1999 XJ36	14.2	3.9	0.919	0.138	0.434	0.079	0.661	0.060		0.344	0.090	0.47	0.30
24750	Ohm	15.0	2.7	0.874	0.071	0.504	0.061	0.878	0.044				0.98	0.17
25106	Ryoojungmin	14.8	3.0	0.902	0.020	0.433	0.016	0.762	0.018				0.68	0.05
26334	1998 WD15	14.9	2.8	0.916	0.012	0.451	0.012	0.802	0.012				0.81	0.04
26873	1994 AP7	14.7	3.1	0.736	0.195	0.429	0.090	0.930	0.086	0.424		0.164	0.85	0.49
26970	Elias	15.1	2.6	0.826	0.025	0.438	0.022	0.739	0.026				0.50	0.08

Number	Name	H	D(km)	B-V	σ_{B-V}	V-R	σ_{V-R}	V-I	σ_{V-I}	V-z'	V-Gunn z	σ_{V-z}	Slope	σ_{Slope}
27364	2000 EJ14	13.1	6.5	0.878	0.008	0.463	0.009	0.835	0.009				0.85	0.03
27448	2000 GQ6	13.3	5.9	0.972	0.055	0.435	0.052	0.690	0.036	0.399		0.059	0.61	0.13
27449	2000 GD14	14.9	2.8	0.878	0.033	0.636	0.028	0.740	0.034				0.69	0.10
27502	Stephbecca	14.6	3.3	0.835	0.020	0.440	0.017	0.849	0.020				0.80	0.06
27963	1997 ST2	15.3	2.4	0.747	0.082	0.399	0.087	0.762	0.110				0.40	0.31
28028	1998 DS8	13.2	6.2	1.055	0.107	0.254	0.060	0.922	0.052	0.555		0.050	1.26	0.24
28221	1998 YG17	14.5	3.4	0.904	0.014	0.425	0.013	0.622	0.011				0.35	0.03
28341	Bingaman	13.3	5.9	0.835	0.042	0.411	0.032	0.807	0.028	0.572		0.045	0.68	0.11

Number	Name	H	D(km)	B-V	σ_{B-V}	V-R	σ_{V-R}	V-I	σ_{V-I}	V-z'	V-Gunn z	σ_{V-z}	Slope	σ_{Slope}
28342	1999 FB9	13.5	5.4	0.945	0.050	0.447	0.036	0.979	0.029	0.467		0.032	1.36	0.13
28665	2000 GN51	15.0	2.7	0.826	0.021	0.426	0.020	0.317	0.025				-0.36	0.06
28707	2000 GZ94	15.3	2.4	0.872	0.023	0.469	0.019	0.740	0.024				0.60	0.07
28747	2000 GF151	15.5	2.2	0.985	0.039	0.476	0.029	0.371	0.033				0.003	0.08
28833	2000 JB35	14.9	2.8	0.910	0.101	0.523	0.080	0.926	0.086				1.18	0.30
28853	2000 JX55	14.1	4.1	0.578	0.217	0.810	0.199	1.061	0.240	0.775		0.313	1.16	0.96
29050	3333 T-2	15.1	2.6	0.811	0.016	0.465	0.009	0.769	0.015				0.56	0.05
29211	1991 RY15	13.0	6.8	0.834	0.040	0.395	0.038	0.907	0.037	0.161		0.057	0.94	0.13

Number	Name	H	D(km)	B-V	σ_{B-V}	V-R	σ_{V-R}	V-I	σ_{V-I}	V-z'	V-Gunn z	σ_{V-z}	Slope	σ_{Slope}
30172	2000 GZ71	14.6	3.3	0.657	0.113	0.409	0.084	1.087	0.082	0.818		0.130	1.19	0.38
30254	2000 HZ25	14.9	2.8	0.234	0.411	0.118	0.211	1.116	0.161	2.105		0.218	0.14	1.41
30286	2000 HG61	15.1	2.6	1.019	0.046	0.507	0.037	0.788	0.035				0.96	0.11
30305	Severi	13.5	5.4	0.881	0.048	0.413	0.032	0.741	0.030	0.489		0.100	0.59	0.12
30563	2001 OZ75	14.8	3.0	0.907	0.016	0.442	0.014	0.617	0.014				0.35	0.04
32323	2000 QW60	14.1	4.1	0.951	0.068	0.370	0.058	0.989	0.063				1.36	0.22
34720	2001 PH54	15.0	2.7	0.787	0.093	0.496	0.084	0.489	0.111				-0.09	0.28
35249	1995 WQ3	14.8	3.0	0.786	0.068	0.451	0.038	0.945	0.041				0.99	0.19

Number	Name	H	D(km)	B-V	σ_{B-V}	V-R	σ_{V-R}	V-I	σ_{V-I}	V-z'	V-Gunn z	σ_{V-z}	Slope	σ_{Slope}
35251	1995 YE5	15.5	2.2	0.931	0.154	0.386	0.116	0.910	0.080				1.10	0.33
35555	1998 FC120	14.5	3.4	0.893	0.016	0.450	0.020	1.001	0.018				1.35	0.06
36518	2000 QC77	15.0	2.7	0.962	0.093	0.435	0.102	0.716	0.092				0.66	0.27
36600	2000 QP138	14.3	3.8	0.906	0.056	0.374	0.065	0.669	0.064				0.44	0.17
36609	2000 QD144	14.9	2.8	0.940	0.106	0.506	0.071	0.600	0.061				0.40	0.21
37361	2001 UW46	14.7	3.1	0.492	0.296	0.693	0.195	0.507	0.157				-0.54	0.76
37411	2001 XH152	15.7	2.0	0.951	0.188	0.490	0.104	0.547	0.105				0.30	0.36
39145	2000 WU90	14.8	3.0	0.926	0.083	0.465	0.050	0.686	0.052				0.55	0.20

Number	Name	H	D(km)	B-V	σ_{B-V}	V-R	σ_{V-R}	V-I	σ_{V-I}	V-z'	V-Gunn z	σ_{V-z}	Slope	σ_{Slope}
39684	1996 PD8	14.7	3.3	0.259	0.133	0.399	0.098	0.825	0.095	0.698		0.186	-0.56	0.48
43996	1997 QH	14.7	3.1	0.762	0.018	0.481	0.013	0.491	0.016				-0.14	0.05
45508	2000 BN18	14.4	3.6	0.895	0.017	0.489	0.013	0.917	0.014				1.12	0.05
45610	2000 DJ48	14.4	3.6	0.813	0.013	0.445	0.011	0.753	0.012				0.52	0.04
45654	2000 EV71	15.9	1.8	0.911	0.073	0.537	0.056	0.774	0.053				0.78	0.18
45695	2000 ET150	14.5	3.4	0.878	0.015	0.449	0.012	0.996	0.016				1.31	0.06
46193	2001 FW141	15.2	2.5	0.817	0.035	0.548	0.024	0.901	0.027				0.97	0.10
46321	2001 QO84	13.9	4.5	0.676	0.077	0.509	0.068	0.927	0.054				0.77	0.22

Number	Name	H	D(km)	B-V	σ_{B-V}	V-R	σ_{V-R}	V-I	σ_{V-I}	V-z'	V-Gunn z	σ_{V-z}	Slope	σ_{Slope}
187223	2005 SX139	16.8	1.2	0.309	0.115	0.446	0.084	0.613	0.065				-0.91	0.35
250694	2005 QX122	16.2	1.6	0.968	0.029	0.474	0.036	0.950	0.022				1.32	0.08

(167) Urda

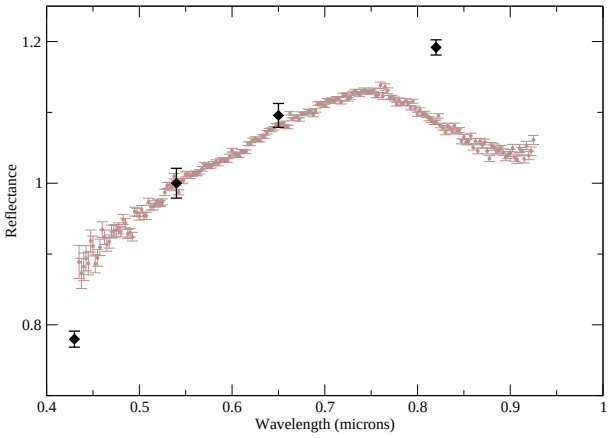

(720) Bohlinia

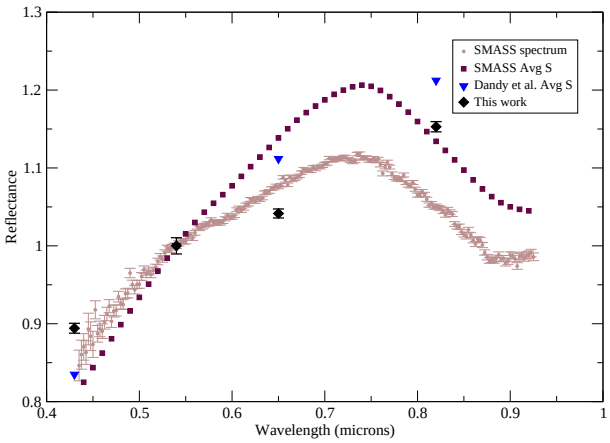

(1336) Zeelandia

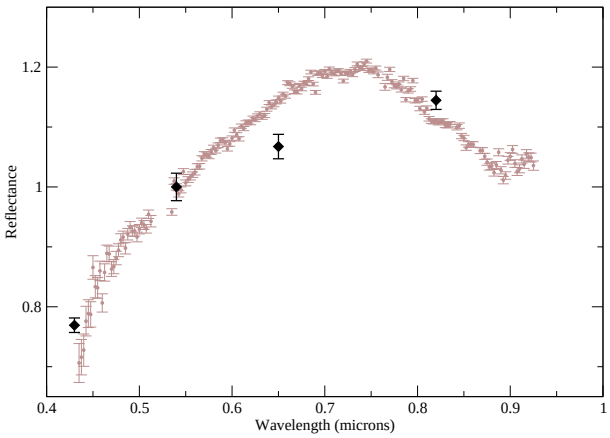

Fig. 1.

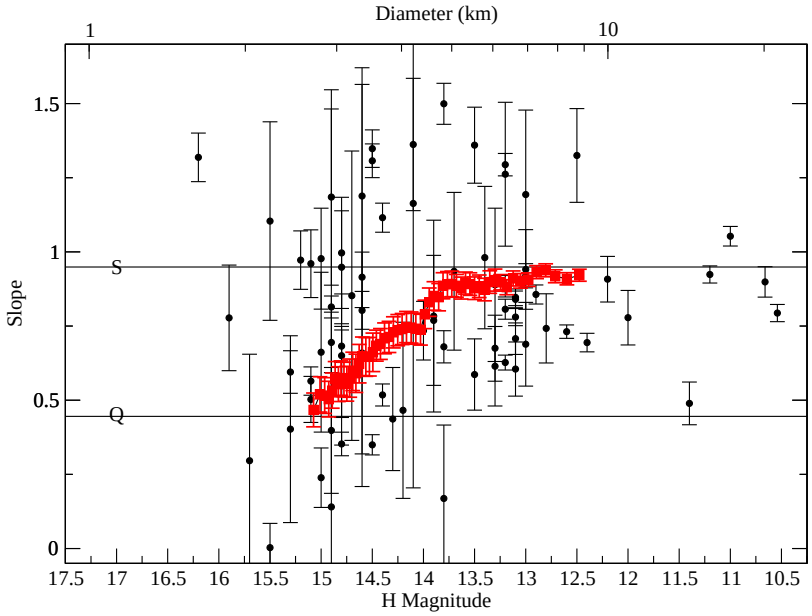
Diameter (km)
1
10
1.5
1
0.5
0
S
Q
Slope
17.5
17
16.5
16
15.5
15
14.5
14
13.5
13
12.5
12
11.5
11
10.5
H Magnitude

Fig. 2.

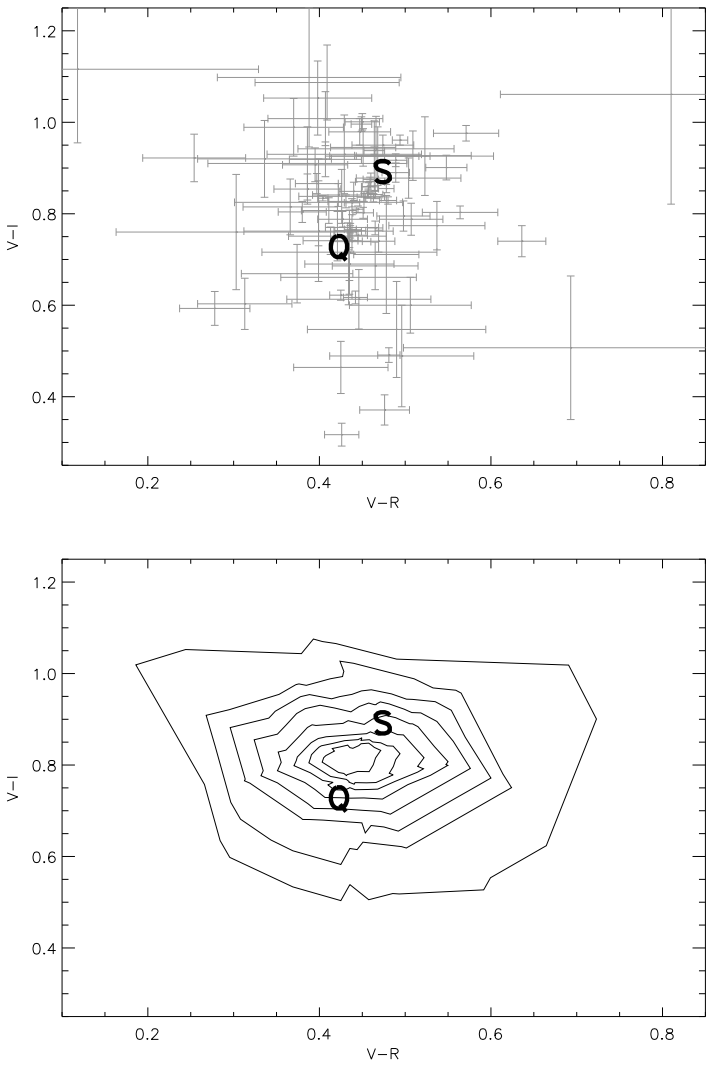

Fig. 3.